Dalton Transactions

ROYAL SOCIETY OF CHEMISTRY

PAPER

View Article Online
View Journal | View Issue

Open Access Article. Published on 31 1399. Downloaded on 28/06/1403 06:59:18 ..
This article is licensed under a Creative Commons Attribution 3.0 Unported Licence.

Check for updates

Cite this: *Dalton Trans.*, 2020, **49**, 12662

Ambidentate bonding and electrochemical implications of pincer-type pyridylidene amide ligands in complexes of nickel, cobalt and zinc†

Philipp Melle, Nathalie Ségaud and Martin Albrecht *

Pincer-type tridentate pyridyl bis(pyridylidene amide) ($pyPYA_2$) ligand systems were coordinated to the Earth-abundant first row transition metals nickel, cobalt and zinc. A one-pot synthesis in water/ethanol afforded octahedral homoleptic bis-PYA complexes, $[M(pyPYA_2)_2](PF_6)_2$, whereas five-coordinate mono-PYA dichloride complexes, $[M(pyPYA_2)Cl_2]$, were obtained upon slow addition of the ligand to the metal chlorides in DMF. Electrochemical measurements further revealed a facile oxidation of the metal centers from Ni^{2+} to Ni^{4+} and Co^{2+} to Co^{3+}, respectively, while the Zn^{2+} system was redox inactive. These experiments further allowed for quantification of the much stronger electron donor properties of neutral *N*,*N*,*N*-tridentate $pyPYA_2$ pincer ligands as compared to terpy. Remarkably, *ortho*-PYA pincer ligands feature amide coordination to the metal center *via* oxygen or nitrogen. This ambidentate ligand binding constitutes another mode of donor flexibility of the PYA ligand system, complementing the resonance structure dynamics established previously. NMR spectroscopic and MS analysis reveal that the *meta*-PYA ligand undergoes selective deuteration when coordinated to cobalt. This reactivity suggests the potential of this ligand as a transient proton reservoir for HX bond activation and, moreover, indicates the relevance of several resonance structures and therefore supports the notion that *meta*-PYA ligands are mesoionic.

Received 14th July 2020,
Accepted 21st August 2020

DOI: 10.1039/d0dt02482a

rsc.li/dalton

Introduction

The large-scale production of bulk chemicals requires the utilization of inexpensive materials, and many industrially relevant processes rely on heterogeneous catalysts based on Earth-abundant metals. Prominent examples are the iron oxide catalysts used in the Haber–Bosch process,[1–3] nickel catalysts in steam reforming for the production of syngas[4–6] or RANEY® nickel catalysts utilized in hydrogenation reactions.[7,8] In contrast, the development of homogeneous catalysts has long focused on complexes based on platinum group and coinage metals.[9] These noble metals feature excellent reactivity and stability properties, though their high price[10] and scarcity[11,12] as well as the high toxicity[13] demand for more sustainable solutions and have led to extensive research activities aiming for the replacement of noble metals by first row transition metals.[14] As a consequence, iron catalysis has made major progress over the last years,[15] including for example the development of highly efficient hydrogenation catalysts that are competitive with the best ruthenium catalysts.[16] Likewise manganese(I) pincer complexes have been explored as attractive alternative to established ruthenium- and iridium-based catalysts in (de)hydrogenation as well as in C–C and C–X bond-forming reactions.[17] Also nickel complexes have gained much attention recently, *e.g.* as low-cost replacement for palladium in cross-coupling reactions.[18]

We have recently developed a new pincer platform based on pyridylidene amide (PYA) ligands (**A**, Fig. 1), which imparted high catalytic activity to ruthenium centers in transfer hydrogenation catalysis.[19,20] Based on the relatively hard yet formally neutral amide donor site of these PYA ligands, we sought to expand the application of this ligand system towards first row transition metals in view of providing a more sustainable alternative to noble metals. PYA ligands have been shown to induce attractive catalytic properties to iridium, ruthenium[21–26] and palladium[27] complexes, in parts by stabilizing high-valent oxidation states and in other parts due to their unique electron donor flexibility.[28–30] Despite these attractive features, no first row transition metal complexes with PYA ligands have been reported, but analogous pyridylidene amine (PYE) ligands have been coordinated to nickel centers by the groups of Johnson[31] and Douthwaite[32] (**B** and **C**, Fig. 1). Here we report nickel, cobalt, and zinc complexes con-

Department für Chemie und Biochemie, Universität Bern, Freiestrasse 3, CH-3012 Bern, Switzerland. E-mail: martin.albrecht@dcb.unibe.ch

† Electronic supplementary information (ESI) available: Crystallographic details, IR and NMR spectra, electrochemical analyses, synthetic details for the Ru complex. CCDC 2015875–2015883. For ESI and crystallographic data in CIF or other electronic format see DOI: 10.1039/d0dt02482a

This journal is © The Royal Society of Chemistry 2020

Open Access Article. Published on 31 1399. Downloaded on 28/06/1403 06:59:18 ..
This article is licensed under a Creative Commons Attribution 3.0 Unported Licence.

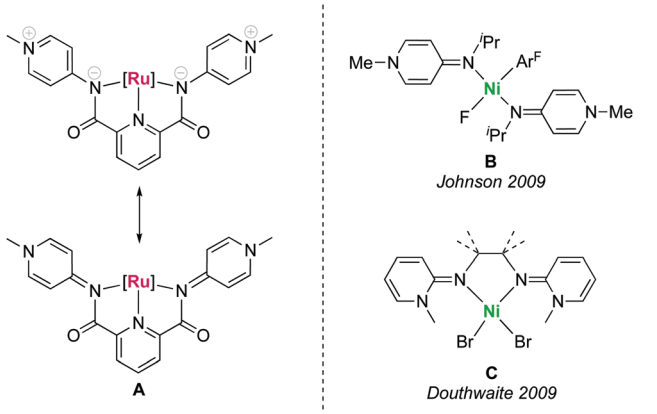

Fig. 1 Pincer pyridylidene amide (PYA) ruthenium complex **A** with two limiting PYA resonance structures, and pyridylidene amine (PYE) nickel complexes **B** and **C** reported earlier.

taining the pyridyl bis(PYA) ($pyPYA_2$) pincer ligand and disclose some unique reactivity properties, including the linkage isomerism between *N*- to *O*-coordination of the PYA ligand as well as isotope exchange reactions at the *meta*-PYA unit that support a mesoionic notion of this ligand.

Results and discussion

Synthesis and characterization of bis(PYA-pincer) complexes

The known *para*- and *meta*-$pyPYA_2$ ligand precursor salts **1a** and **1b** were prepared according to standard procedures.[19,33] Similarly, the *ortho*-$pyPYA_2$ ligand precursor **1c** was prepared from 2-aminopyridine and 2,6-pyridinedicarbonyl dichloride followed by selective methylation of both aminopyridine sites and anion metathesis. Notably, methylation required an excess of MeOTf (5 eq.) to be quantitative, while the use of MeI, which was sufficient for methylation of the *para* and *meta* analogues, resulted in only partial methylation. Complexation to cobalt and nickel was accomplished by reacting the dicationic ligand salts **1a–c** with the corresponding chloride salt ($CoCl_2$, $NiCl_2$) in the presence of Na_2CO_3 as a base (Scheme 1). Complexation under these conditions consistently afforded the octahedral homoleptic complexes $[M(pyPYA_2)_2](PF_6)_2$ (M = Co, **2a–c**; M = Ni, **3a–c**) even when a large excess of the metal salt was used. This reactivity pattern contrasts the analogous ruthenation, which exclusively afforded mono-ligated $[Ru(pyPYA_2)(MeCN)_3]^{2+}$ complexes. Complexes **2** and **3** are paramagnetic and NMR silent, their quantitative elemental composition, structure and purity was therefore confirmed by CHN microanalysis, single crystal X-ray diffraction, and HR ESI-MS. The latter showed the monocationic complex fragments $[M - PF_6]^+$, *e.g.* at 898.1733 amu for **2a** (calcd 898.1733).

Crystallographic analysis revealed ambidentate coordination of the *ortho*-$pyPYA_2$ ligand in **2c** and **3c**, as one of the ligands is bound to the metal center in the typical κ^3-*N*,*N*,*N* bonding mode, while the other ligand binds with the amide through oxygen in a κ^3-*O*,*N*,*O* coordination mode (*cf.* Scheme 1, Table S1, Fig. S1†). Both *meta*-$pyPYA_2$ ligands in complexes **2b** and **3b** show the expected κ^3-*N*,*N*,*N* coordination through the amide nitrogens and the central pyridine as observed for related dianionic pyridine dicarboxamidate

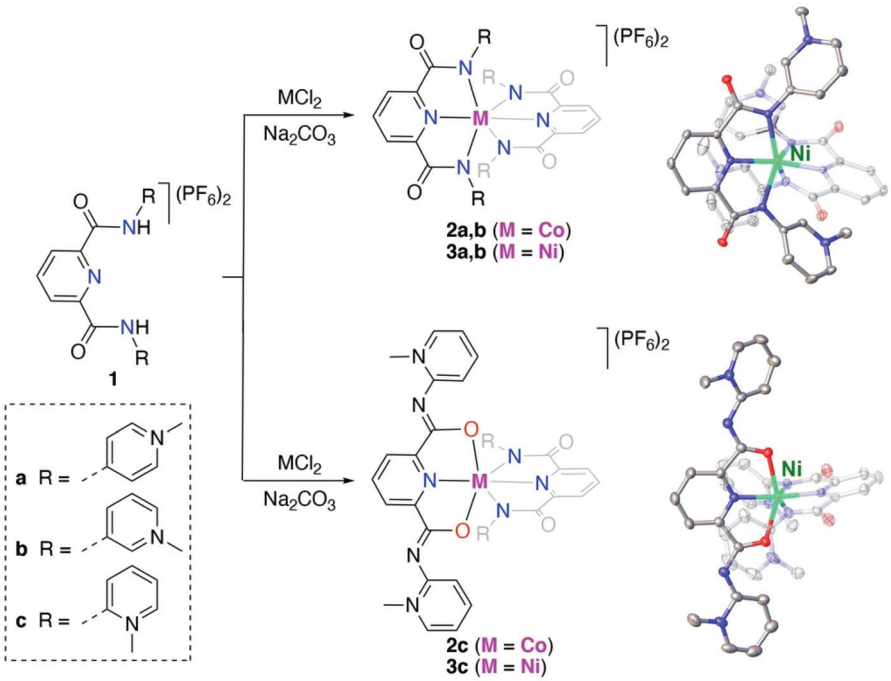

Scheme 1 Synthesis of Co(II) and Ni(II) bis-$pyPYA_2$ pincer complexes **2a–c** and **3a–c** in H_2O/EtOH (1 : 1 v/v). Crystal structures of complex cations **3b** and **3c**; all ellipsoids at 50% probability level (hydrogen atoms and co-crystallized solvent molecules omitted for clarity).

Open Access Article. Published on 31 1399. Downloaded on 28/06/1403 06:59:18 ..
This article is licensed under a Creative Commons Attribution 3.0 Unported Licence.

systems.[34–36] Such a linkage isomerism of PYA ligands has been proposed,[37] yet never established so far[38] and presents a further type of flexibility of the PYA system. Notably, the same *ortho*-pyPYA$_2$ ligand displayed the classic κ^3-*N*,*N*,*N*-coordination mode when bound to ruthenium(II) in [Ru(*ortho*-pyPYA$_2$)(MeCN)$_3$](PF$_6$)$_2$ (Fig. S2†). Likewise, pyridine dicarboxamide systems with *ortho*-dimethylated aryl substituents show exclusively κ^3-*N*,*N*,*N*-bonding.[35,39] The κ^3-*O*,*N*,*O* coordination mode is unprecedented and presumably a consequence of the Lewis acidity of the first row transition metal centers and their ensuing oxophilicity, combined with the unique donor flexibility of the formally neutral and sterically constrained *ortho*-PYA donor site, and distinguishes these ligands from the more commonly used pyridine carboxamide systems.

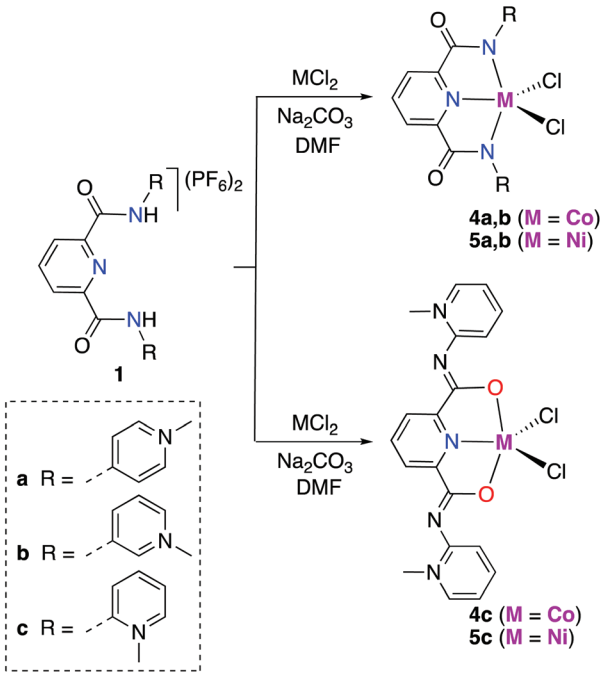

Scheme 2 Synthesis of Ni(II) and Co(II) [M(pyPYA$_2$)Cl$_2$] complexes **4a–c** and **5a–c** by slow addition of deprotonated ligand at room temperature.

Synthesis and characterization of mono(PYA-pincer) complexes

The synthesis of cobalt and nickel mono-PYA complexes, [M(pyPYA$_2$)Cl$_2$] complexes **4a–c** (M = Co) and **5a–c** (M = Ni; Scheme 2), was accomplished by slow addition of a filtered DMF solution containing the ligand and Na$_2$CO$_3$ to a DMF solution containing the metal chloride. The slow addition of ligand as well as the choice of solvent played a crucial role. Initial attempts to control the reaction of the PYA ligands **1a–c** with MCl$_2$ by quenching the reaction at early reaction times or by using a large excess of the metal salt (up to 10 eq.) invariably resulted in the formation of the homoleptic [M(pyPYA$_2$)$_2$]$^{2+}$ compounds **2** and **3**.

Formation of complexes **4** and **5** was established by CHN microanalysis as well as HR ESI-MS, which showed the monocationic complex fragments [M − Cl]$^+$, *e.g.* at 441.0409 amu for **4a** (calcd 441.0403). The set of cobalt complexes **4a–c** was furthermore characterized by single crystal X-ray diffraction analysis (Fig. 2). The complexes feature a strongly distorted trigonal bipyramidal arrangement (τ_5 = 0.45–0.49),[40] which is in good agreement with the reported analogous structure of [Co(terpy)Cl$_2$] (terpy = terpyridine).[41] The *para*- and *meta*-PYA pincer ligands in complexes **4a,b** bind to the metal center in a κ^3-*N*,*N*,*N* coordination mode whereas the *ortho*-PYA pincer ligand in **4c** is again κ^3-*O*,*N*,*O* coordinated as observed for the bis-PYA pincer complexes. Notably, steric constraints should be less relevant when the PYA pincer ligand is bound to the CoCl$_2$ fragment than in bis-PYA pincer complexes, indicating an electronic stabilization of the PYA coordination through oxygen.

The *para*- and *meta*-PYA pincer ligands in complexes **4a,b** are almost planar, *i.e.* the dihedral angle between the PYA heterocycles and central pyridine ring are only 8.5°, 9.8° in **4a** and

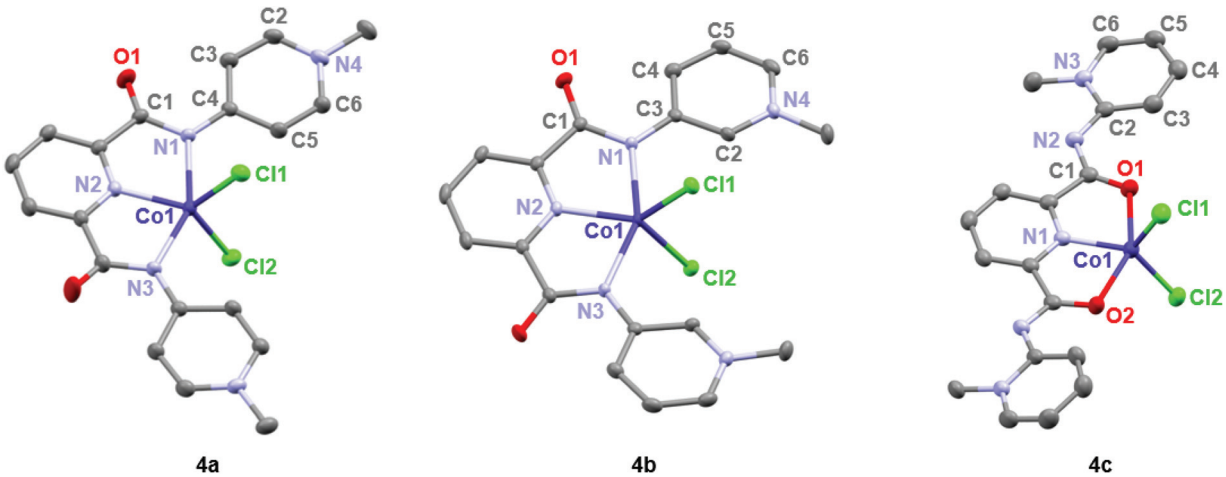

Fig. 2 ORTEP representations of mono-pyPYA$_2$ cobalt complexes **4a–c**; all ellipsoids at 50% probability level (hydrogen atoms and co-crystallized solvent molecules omitted for clarity).

Open Access Article. Published on 31 1399. Downloaded on 28/06/1403 06:59:18 ..
This article is licensed under a Creative Commons Attribution 3.0 Unported Licence.

Table 1 Selected bond lengths (Å) and angles (°) of mono-pyPYA$_2$ complex cations **4a–c**

	4a	4b		4c
Co1–N1	2.227(2)	2.185(1)	Co1–O1	2.217(2)
Co1–N2	2.020(2)	2.005(1)	Co1–N1	2.018(1)
Co1–N3	2.217(2)	2.185(1)	Co1–O2	2.225(2)
Co1–Cl1	2.315(1)	2.330(1)	Co1–Cl1	2.249(1)
Co1–Cl2	2.296(1)	2.330(1)	Co1–Cl2	2.262(1)
N1–C1[a]	1.360(3)	1.347(2)	N2–C1[a]	1.331(3)
C1–O1[a]	1.231(2)	1.244(2)	C1–O1[a]	1.254(2)
N1–C3/4[a]	1.373(2)	1.391(2)	N2–C2[a]	1.353(3)
C3–C4[a]	1.412(3)	1.406(2)	C2–C3[a]	1.405(3)
C4–C5[a]	1.419(3)	1.388(2)	C3–C4[a]	1.368(4)
C5–C6[a]	1.364(3)	1.366(2)	C4–C5[a]	1.393(4)
C6–N4[a]	1.345(3)	1.349(2)	C5–C6[a]	1.353(3)
N4–C2[a]	1.353(2)	1.342(2)	C6–N3[a]	1.356(3)
C2–C3[a]	1.365(3)	1.399(2)	N3–C2[a]	1.375(3)
N1–Co1–N3	153.1(1)	154.1(1)	O1–Co1–O2	152.0(2)
θ PYA-pyr[b]	8.5 & 9.8	10.4 & 10.4	θ PYA-pyr[b]	11.3 & 25.8
τ_5[c]	0.46	0.49	τ_5[c]	0.45

[a] Average of two bonds. [b] Dihedral angle θ between the PYA heterocycles and the pyridyl-amide plane. [c] See ref. 40.

10.4° in **4b** respectively (Table 1), which is distinctly different when compared to the correspondent homoleptic complex variation [Co(*meta*-pyPYA$_2$)$_2$](PF$_6$)$_2$ which show a 55° twist between the PYA and central pyridyl planes. This high planarity may hint to a significant π-contribution of the N_{amide}–C_{PYA} bonds (N1–C3/4) in both complexes. In such a model, the amide nitrogen is acting predominantly as neutral L-type N-donor ligand, presumably as a consequence of the higher electron density at the formally neutral metal center in complexes **4** and **5** compared to the dicationic center in the bis (pincer) complexes **2** and **3**. In agreement with a more pronounced L-type and π-acidic binding mode of the amide nitrogen, the *para*-PYA heterocycles of complex **4a** reveal a pronounced diene-imine resonance form with localized double and single bonds (average C2–C3 and C5–C6 1.365(4) Å, average C3–C4 and C4–C5 bonds (1.415(7) Å; Table 1). This bond alteration implies considerable contribution of the imine resonance structure of the PYA unit (*cf.* bottom structure of **A** in Fig. 1).

The κ^3-*O*,*N*,*O* coordination mode of the *ortho*-PYA pincer ligand in mono-pyPYA$_2$ complex **4c** suggests this complex to be an intermediate *en route* to the formation of the heteroleptic bis-pyPYA$_2$ pincer complex **2c**. The stronger coordination of the *O*,*N*,*O* donor set may then accommodate a second PYA pincer ligand in the more typical κ^3-*N*,*N*,*N* mode.

Dynamic linkage isomerism of the *ortho*-PYA-pincer ligand system

For better spectroscopic analysis in solution, the analogous zinc(II) complexes [Zn(pyPYA$_2$)$_2$](PF$_6$)$_2$ **6a–c** were prepared by reacting ligands **1a–c** with 0.5 eq. ZnCl$_2$ under mildly basic conditions (Scheme 3). In contrast to the paramagnetic and NMR-silent octahedral Co(II) and Ni(II) complexes **2** and **3**, complexes **6a–c** are diamagnetic and allow for NMR spectroscopic characterization. Ligand coordination to the Zn^{II} center resulted in the loss of the NH amide proton resonances and in a marked upfield shift of the aromatic H_{PYA} proton resonances, *e.g.* from δ_H = 9.76 ($H^6{}_{PYA}$) in *meta*-PYA ligand **1b** to δ = 8.43 in complex **6b**.

All zinc complexes **6a–c** feature one distinct set of PYA ligand proton resonances, including N-CH$_3$ (δ_H around 4), pyridyl (δ_H 8.25–8.70) and pyridylidene (δ_H 7.08–8.43) signals. This symmetric arrangement indicates that both pyPYA$_2$ ligands in each zinc complex are coordinated in the same mode, most presumably the typical κ^3-*N*,*N*,*N*-coordination based on the structures of the cobalt and nickel analogues and previously described structures.[19,42–45]

The symmetric ligand bonding in **6c** containing *ortho*-pyPYA$_2$ ligands contrasts the solid state bonding established for the analogous nickel and cobalt complexes **2c** and **3c** comprised of a mixture of κ^3-*N*,*N*,*N* and κ^3-*O*,*N*,*O* pincer coordination. NMR spectroscopic analysis of complex **6c** at low temperature indicated decoalescence of the signals into two sets in a 9 : 1 integral ratio, indicating the presence of two species (Fig. 3). Based on the six inequivalent aromatic resonances, the major species was assigned to the homoleptic bis-κ^3-*N*,*N*,*N*-coordinated pincer isomer. The minor isomer features at least ten inequivalent proton signals, which were therefore attributed to mixed κ^3-*N*,*N*,*N*/κ^3-*O*,*N*,*O*-coordination isomer (*cf.* structures of **2c**, **3c**). These measurements therefore suggest that at room temperature, complex **6c** undergoes rapid κ*N*-/κ*O*-amide isomerization.

The dynamic process of this complex was investigated by variable temperature ^{1}H NMR spectroscopic experiments in CD$_2$Cl$_2$ in the +20 to −80 °C temperature range (Fig. S3†). Decoalescence of most of the pyridyl and PYA proton resonances was observed around −40 °C, apart from the PYA H^6

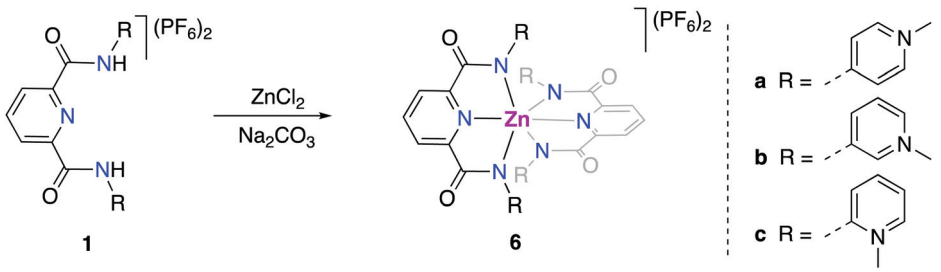

Scheme 3 Synthesis of [Zn(pyPYA$_2$)$_2$](PF$_6$)$_2$ complexes **6a–c**. (a) 0.5 eq. ZnCl$_2$; 3 eq. Na$_2$CO$_3$ in MeCN.

Open Access Article. Published on 31 1399. Downloaded on 28/06/1403 06:59:18 ..
This article is licensed under a Creative Commons Attribution 3.0 Unported Licence.

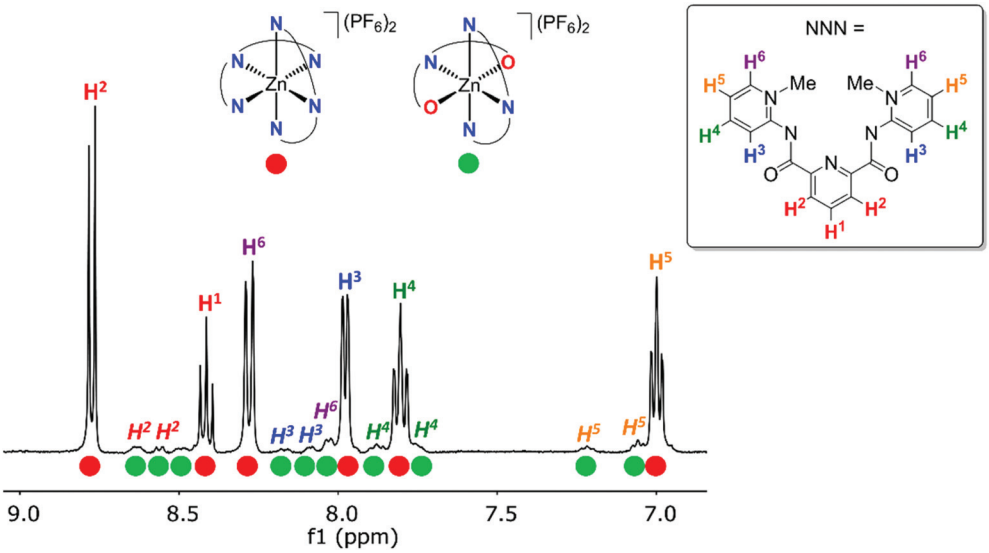

Fig. 3 ^{1}H NMR spectrum of [Zn(*ortho*-pyPYA$_2$)$_2$](PF$_6$)$_2$ **6c** in CD$_2$Cl$_2$ at −80 °C, revealing two different complexes in 9 : 1 ratio. The major species was assigned to the bis-(κ^3-*N,N,N*)-coordination isomer (red circles), the minor species to the mixed κ^3-*N,N,N*/κ^3-*O,N,O*-coordination isomer (green circles).

signal, which undergoes the largest shift and features a coalescence temperature T_c around −20 °C. Based on these values and applying the Eyring equation, an average activation energy $\Delta G^{\ddagger}$ = 11.4 ± 0.3 kcal mol^{-1} was calculated for this PYA linkage isomerism (Table S2†).[46,47] A similar behavior was noted in CD$_3$CN (Fig. S4†), though due to the higher melting point of this solvent, the decoalescence was not resolved. Nonetheless, these experiments suggest that the dynamic bonding is not significantly depending on the solvent.

The bonding mode in the bis-(pyPYA$_2$) complexes was further analyzed by solid state infrared (IR) spectroscopy of the pure compounds. The ligand precursor **1a** features three characteristic absorption bands for the amide carbonyl and PYA-imine units in the 1580–1700 cm^{-1} region (Table 2, Fig. S5–S11†).[48] Upon metalation, the two lower bands around 1590 and 1645 cm^{-1} remain essentially unchanged, while the high energy band at 1706 cm^{-1} shifts characteristically to 1617 (±1) cm^{-1}, presumably due to metal coordination to the amide unit (Fig. 4a). Likewise, the strong absorption above 1700 cm^{-1} for ligand precursors **1b** and **1c** shifts to lower energy upon metalation, though assignments are more complicated as all bands shift considerably (Fig. 4b and Fig. S5†). It is worth noting that the shift is independent of the metal center and that the IR spectra are essentially identical for Co(II), Ni(II), and Zn(II) complexes for the *para*- and *meta*-pyPYA$_2$ ligand even in the low frequency area. This high similarity suggests an identical coordination mode for all three metal complexes. For the *ortho*-pyPYA$_2$ series, however, subtle differences are noted in the 1550–1650 cm^{-1} range which distinguish the Zn from the Ni and Co systems (Fig. 4c). These differences may point to a different ligand behavior, which may be associated with the κ^3-*N,N,N vs.* κ^3-*O,N,O* linkage isomerism established

Table 2 Characteristic IR stretch frequencies of all compounds in the carbonyl/imine range between 1580–1700 cm^{-1} and redox potentials of all compounds

Entry	Ligand motif	Bonding partner		$\nu_{C=O/C=N}$ [cm^{-1}]	$E_{1/2}$ (M$^{II/III}$)^a [V]	$E_{1/2}$ (M$^{III/IV}$)^a [V]
1	*para*-PYA	H	**1a**	1593, 1646, 1706	—	—
2	*para*-PYA	Co	**2a**	1586, 1617, 1642	0.20 (90)	—
3	*para*-PYA	Ni	**3a**	1587, 1617, 1645	1.20 (80)	1.72 (150)
4	*para*-PYA	Zn	**6a**	1584, 1618, 1646	—	—
5	*meta*-PYA	H	**1b**	1695	—	—
6	*meta*-PYA	Co	**2b**	1567	0.01 (80)	—
7	*meta*-PYA	Ni	**3b**	1564	1.03 (80)	1.54 (90)
8	*meta*-PYA	Zn	**6b**	1566	—	—
9	*ortho*-PYA	H	**1c**	1583, 1637, 1721	—	—
10	*ortho*-PYA	Co	**2c**	1597, 1628	0.40 (100)	—
11	*ortho*-PYA	Ni	**3c**	1598, 1627	1.34 (100)	—
12	*ortho*-PYA	Zn	**6c**	1587, 1630	—	—

^{a} Potentials in MeCN *vs.* SSCE at 100 mV s^{-1} scan rate using the Fc$^+$/Fc couple as standard; $E_{1/2}$ = +0.43 V and (*n*Bu$_4$N)PF$_6$ as electrolyte, 0–2.2 V sweep range; $\Delta E_p = |E_{pc} - E_{pa}|$ [mV] in parenthesis.

 This journal is © The Royal Society of Chemistry 2020

Open Access Article. Published on 31 1399. Downloaded on 28/06/1403 06:59:18 ..
This article is licensed under a Creative Commons Attribution 3.0 Unported Licence.

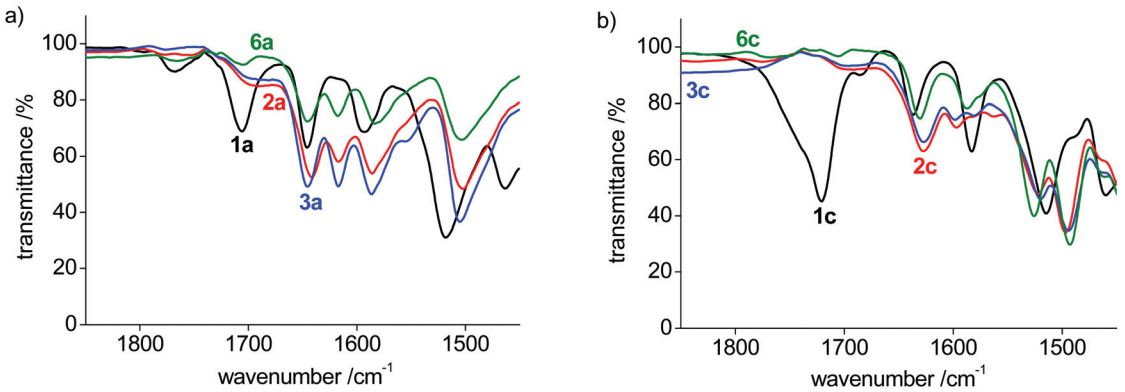

Fig. 4 IR spectra of (a) *para*-pyPYA$_2$ pincer complex series; (b) *ortho*-pyPYA$_2$ pincer complex series.

for the [Zn(*ortho*-pyPYA$_2$)$_2$](PF$_6$)$_2$ complex **6c** by NMR spectroscopy. IR spectroscopy therefore does not conclusively indicate whether this linkage isomerism is exclusively occurring at Zn^{2+}, or whether it is more general for *ortho*-pyPYA$_2$ ligands and also takes place at Co^{2+} and Ni^{2+}. The exclusive κ^3-*O*,*N*,*O* bonding in the solid state of the latter two complexes (*cf.* structures of **2c**–**5c**) might be induced by lower solubility or a preferential crystal packing of the mixed coordination isomer, leading to a dynamic kinetic resolution of the two isomers through crystallization.

Redox properties of homoleptic bis-PYA pincer complexes

The orange *meta*-pyPYA$_2$ cobalt(II) complex **2b** oxidized to the green Co(III) analogue **2b**$^+$ under aerobic conditions in a saturated aqueous solution (Scheme 4). The oxidation state of the cobalt center in **2b**$^+$ was unambiguously identified by crystallographic analysis due to the 0.2 Å shorter Co–N bond distances compared to **2b** as well as the presence of three PF_6^- counter ions. This oxidation under mild conditions indicates strong donor properties of the PYA pincer ligand in these cobalt and nickel complexes. Therefore, the electrochemical properties of the complexes were investigated by cyclic voltammetry.

Cobalt complexes **2a**–**c** show reversible redox processes in the 0 to +0.5 V potential range that were assigned to metal-centered Co^{2+} to Co^{3+} oxidations (all potentials *vs.* Ag/AgCl; Fig. 5). The octahedral complex [Co(terpy)$_2$](PF$_6$)$_2$ [49] was also included to compare the donor strength of the formally neutral tridentate PYA pincer ligands with a well-studied reference compound. The reversibility of the $M^{II/III}$ oxidation processes in complexes **2** and **3** is supported by the linear relationship of anodic (I_{pa}) and cathodic peak currents (I_{pc}) *vs.* the square root of the scan rate (Fig. S12†). This linearity together with the small peak potential difference ΔE_p < 105 mV (Table 2) indicates a diffusion limited electron transfer process.[50–52] The oxidation potential is dependent on the PYA substitution pattern and is lowest for cobalt coordinated to the *meta*-PYA pincer ligand ($E_{1/2}$ = 0.01 V in **2b**) and increases with *para*-PYA ($E_{1/2}$ = 0.20 V in **2a**)[53] and even more with *ortho*-PYA pincer ligands ($E_{1/2}$ = 0.40 V in **2c**). It is noteworthy that [Co(*ortho*-pyPYA$_2$)$_2$](PF$_6$)$_2$ complex **2c** features two consecutive redox processes in the potential range of 0.3–0.6 V, which might be caused by possible linkage isomerism in solution and the presence of two coordination isomers (exclusively κ^3-*N*,*N*,*N*-coordinated ligand and mixed coordination mode, *cf.* NMR studies of analogous *ortho*-PYA zinc complex above). These half wave potentials indicate an increase of ligand donor strength along the series *ortho*-PYA < *para*-PYA < *meta*-PYA, a trend that has been previously observed for [Ru(pyPYA$_2$)L$_3$]$^{2+}$ and [IrCp*(phenyl-PYA)L]$^+$ complexes.[19,54] This trend points to a strongly π-basic character of the *meta*-PYA donor, while the donor properties of the *ortho*-PYA unit are probably attenuated by the vicinity of the formally positively charged pyridinium nitrogen. When compared to the redox properties of [Co(terpy)$_2$]$^{2+}$ ($E_{1/2}$ = 0.32 V)[55] the *ortho*-PYA pincer ligand is less donating than terpy,

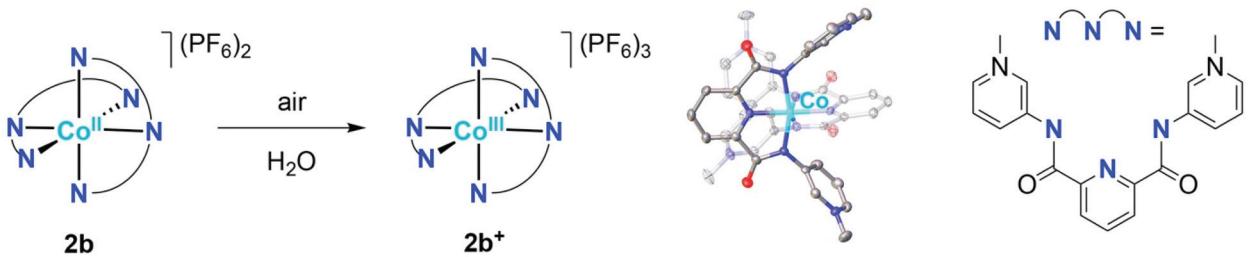

Scheme 4 Oxidation of [Co(*meta*-pyPYA$_2$)$_2$](PF$_6$)$_2$ **2b** in H$_2$O under aerobic conditions, to the Co(III) complex **2b**$^+$. Crystal structure of complex cation **2b**$^+$; all ellipsoids at 50% probability level (hydrogen atoms and co-crystallized solvent molecules omitted for clarity).

Open Access Article. Published on 31 1399. Downloaded on 28/06/1403 06:59:18 ..
This article is licensed under a Creative Commons Attribution 3.0 Unported Licence.

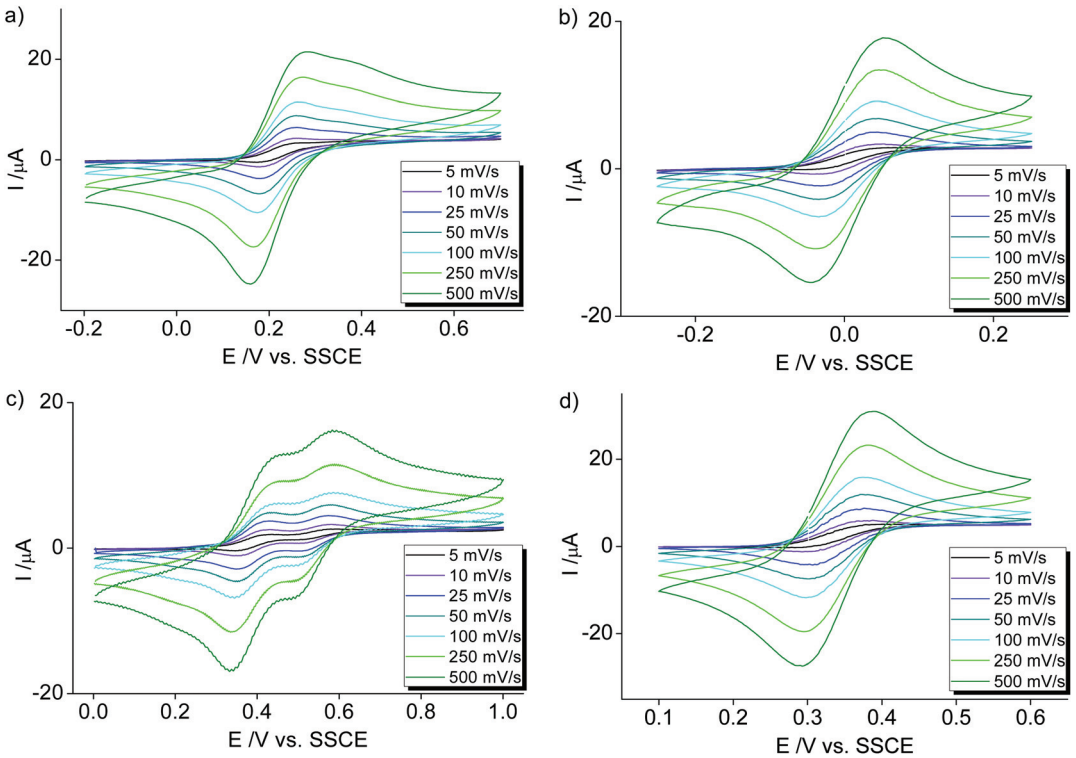

Fig. 5 Cyclic voltammetry measurements of homoleptic $[Co(pyPYA_2)_2](PF_6)_2$ complexes in MeCN: (a) **2a** $[Co(para\text{-}pyPYA_2)_2](PF_6)_2$; (b) **2b** $[Co(meta\text{-}pyPYA_2)_2](PF_6)_2$; (c) **2c** $[Co(ortho\text{-}pyPYA_2)_2](PF_6)_2$; (d) $[Co(terpy)_2](PF_6)_2$. Conditions: 10 mL solvent, 1 mM sample and 100 mM $(nBu_4N)PF_6$ as supporting electrolyte at 5–500 mV s^{-1} scan rate (potentials *vs.* Ag/AgCl using the Fc^+/Fc couple as standard; $E_{1/2}$ = +0.4319).

while the *para* and even more so the *meta* analogue are stronger donors.

The metal-centered nature of the oxidation process was confirmed by redox analyses of the Zn analogues **6a–c**. These complexes do not show any redox activity in the 0–2.2 V potential window (Fig. S14†), indicating that the coordinated PYA pincer ligands are redox inactive within this range. Likewise, the three pyridinium salt ligand precursors **1a–c** do not show any oxidation process up to 2 V and feature an irreversible reduction processes around −1 V (Fig. S13†). This reduction is dependent on the PYA substitution pattern and easiest for *ortho*-PYA system **1c** (E_{pc} = −0.98 V), intermediate for *meta*-PYA **1b** (E_{pc} = −1.22 V) and at lowest potential for the *para* analogue **1a** (E_{pc} = −1.33 V).

Electrochemical characterization of the nickel complexes supports the trend in donor strength of the PYA pincer ligands as observed for the Co series. Thus, the Ni^{3+} oxidation state was stabilized better by the *meta*-PYA pincer ligand ($E_{1/2}$ = 1.03 V in **3b**) than the *para* analogue ($E_{1/2}$ = 1.20 V in **3a**) or the *ortho*-$pyPYA_2$ system ($E_{1/2}$ = 1.34 V in **3c**; Fig. 6a–c). In addition, the stronger donor sets also provided access to Ni^{IV} complexes *via* a second reversible oxidation at higher potential ($E_{1/2}$ = 1.72 V and 1.54 V for complexes **3a** and **3b**, respectively). Notably, $[Ni(terpy)_2](PF_6)_2$ as reference compound is oxidized at considerably higher potential ($E_{1/2}$ = 1.65 V),[55] suggesting weaker donation of the terpy ligand than even the least basic *ortho*-$pyPYA_2$ ligand.

H/D exchange in *meta*-PYA sites

A closer investigation of the homoleptic cobalt complex **2b** with *meta*-PYA pincer ligands revealed intriguing ligand-based reactivity. Crystallization of this complex in D_2O under aerobic conditions resulted in a mixture of orange and green crystals. The latter are a product of spontaneous oxidation of a the metal center and furthermore revealed selective deuterium incorporation into the PYA heterocycle, as demonstrated by MS and NMR analyses. Material crystallized from D_2O showed the *m*/*z* signals for the mono-, di-, and tri-cationic species at 8, 4 and 2.66 amu higher, respectively, than samples of $\mathbf{2b}^+$ crystallized from H_2O (Table S3†). Formation of $\mathbf{2b}^+\text{-}d_8$ was further supported by the absence of the PYA resonances at δ_H 8.11 and 8.25 in the ^1H NMR spectrum of the complex generated in D_2O (Fig. S15†). Based on NOE spectroscopy as well as the pertinent coupling constants, these resonances were assigned to $H^2{}_{PYA}$ and $H^6{}_{PYA}$, respectively, *i.e.* the positions *ortho* to the PYA nitrogen. These data indicate a highly selective H/D exchange. Interestingly, the isomeric complexes **2a** and **2c** containing *para*- and *ortho*-PYA pincer ligands, respectively do not undergo any detectable deuteration or oxidation (MS, NMR) when exposed to D_2O, presumably because of the higher oxidation potential of these complexes (*vide supra*). The selective deuterium incorporation in the PYA 2- and 6-position of **2b** may be rationalized by considering resonance forms **B** and **C** of the *meta*-PYA ligand system, which imply a formally neutral imine donor site and opposite charges within the pyridylidene

 This journal is © The Royal Society of Chemistry 2020

Open Access Article. Published on 31 1399. Downloaded on 28/06/1403 06:59:18 ..
This article is licensed under a Creative Commons Attribution 3.0 Unported Licence.

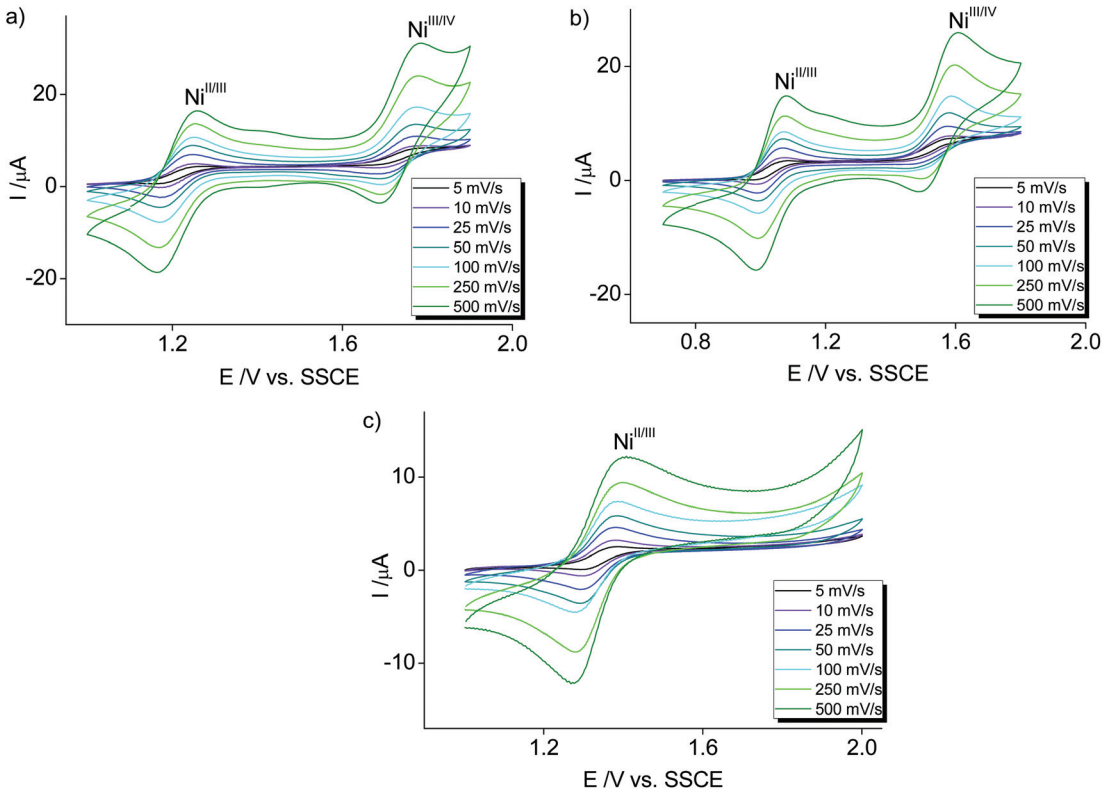

Fig. 6 Cyclic voltammetry measurements of homoleptic $[Ni(pyPYA_2)_2](PF_6)_2$ complexes in MeCN: (a) **3a** $[Ni(\textit{para}\text{-}pyPYA_2)_2](PF_6)_2$; (b) **3b** $[Ni(\textit{meta}\text{-}pyPYA_2)_2](PF_6)_2$; (c) **3c** $[Ni(\textit{ortho}\text{-}pyPYA_2)_2](PF_6)_2$. Conditions: 10 mL solvent, 1 mM sample and 100 mM $(nBu_4N)PF_6$ as supporting electrolyte at 5–500 mV s^{-1} scan rate (potentials *vs.* SSCE using the Fc^+/Fc couple as standard; $E_{1/2}$ = +0.4319).

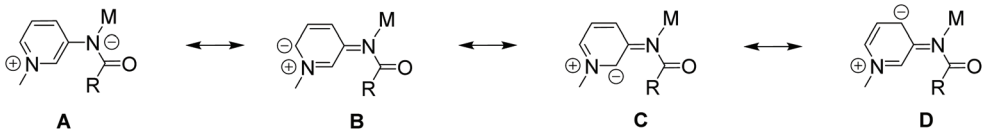

Scheme 5 Limiting resonance structures of the mesoionic *meta*-PYA ligand site. The negative charge is localized on the amide nitrogen and in 2-, 4- and 6-position of the PYA heterocycle.

heterocycle (Scheme 5). Reversible deuteration/protonation at the partially negatively charged positions would account for the observed selectivity and indicates that resonance forms **B** and **C** are contributing in addition to resonane form **A**. This contribution of several resonance structures therefore validates *meta*-PYA systems as mesoionic compounds.[56]

Conclusions

Here, we have shown that PYA pincer ligands form stable complexes with nickel, cobalt and zinc, which expands the application potential of this ligand beyond platinum group metals to first row metals. The substitution pattern of the PYA heterocycle influences the binding mode of the pincer ligand to these Earth-abundant transition metals. *meta*- and *para*-$pyPYA_2$ ligand systems are exclusively κ^3-*N*,*N*,*N*-coordinated, whereas the *ortho*-methylated PYA pincer ligand forms either κ^3-*O*,*N*,*O*-coordinated mono-$pyPYA_2$ compounds or bis-$pyPYA_2$ complexes with a mixed κ^3-*O*,*N*,*O*/κ^3-*N*,*N*,*N* coordination mode. According to electrochemical analyses, the donor strength of the PYA ligand systems decrease in the order *meta*-PYA > *para*-PYA > *ortho*-PYA. The mesoionic *meta*-PYA pincer cobalt complex displays unique reactivity, since the 2- and 6-positions of the pyridinium heterocycle are selectively deuterated in D_2O under mild conditions. This deuteration suggests partial delocalization of the negative charge and therefore mesoionic properties of the *meta*-PYA unit. Moreover, this reactivity may become potentially useful for metal–ligand cooperative HX bond activation catalysis.

Experimental

General

All reagents were commercially available and used as received. Ligands **1a** and **1b** have been prepared according to previously

Open Access Article. Published on 31 1399. Downloaded on 28/06/1403 06:59:18 ..
This article is licensed under a Creative Commons Attribution 3.0 Unported Licence.

described methods.[19] Unless specified otherwise, ^{1}H NMR spectra were recorded at 25 °C on Bruker spectrometers operating at 300 MHz. Chemical shifts (δ in ppm, coupling constants J in Hz) were referenced to residual solvent signals. Assignments are based on homo- and heteronuclear shift correlation spectroscopy. Purity of bulk samples of the complexes has been established by NMR spectroscopy, and when possible by elemental analysis. Elemental analyses were performed at DCB Microanalytic Laboratory using a Thermo Scientific Flash 2000 CHNS-O elemental analyzer. High-resolution ESI mass spectrometry was carried out with a Thermo Scientific LTQ Orbitrap XL (ESI-TOF). Cyclic voltammograms were recorded using an Autolab PGSTAT101 from Metrohm in MeCN solutions: 10 mL solvent, 1 mM sample and 100 mM tetrabutylammonium hexafluorophosphate (nBu$_4$N)PF$_6$ as supporting electrolyte. Solutions were deaerated with argon gas for 10 min prior to each run. The scan rate was 100 mV s^{-1}. Redox potentials were measured using a Pt-button working electrode, an Ag/AgCl reference electrode and a Pt-wire auxiliary electrode and are tabulated *versus* a ferrocene internal standard. The Fc$^+$/Fc couple is 0.43 V *vs.* Ag/AgCl in 0.1 M (nBu$_4$N)PF$_6$ MeCN solutions.[57] ATR-FTIR spectra were recorded with a Jasco FT/IR-4700 spectrometer with a Jasco ATR Pro One unit containing a diamond crystal.

Synthetic procedures

Compound 1c. The bis-amide N^2,N^6-bis(pyridin-2-yl)pyridine-2,6-dicarboxamide has been prepared according to literature procedures.[33] Methylation was carried out under nitrogen atmosphere in 1,2-dichloroethane (50 mL) at 80 °C under vigorous stirring for 3 days with 5 eq. MeOTf (1.64 g; 10 mmol) in respect to the bis-amide (640 mg; 2 mmol). The reaction was quenched with MeOH (5 mL) and the product precipitated upon addition of Et$_2$O (50 mL). It was purified by filtration and repetitive washing with Et$_2$O (3 × 50 mL), yielding the bis-methylated OTf ligand salt **pre-1c** (1.03 g; 79% yield). The final product was obtained after anion exchange to PF$_6$, which was achieved upon addition of 4 eq. NH$_4$PF$_6$ (1.04 g; 6.3 mmol) to a solution of **pre-1c** (1.03 g; 1.6 mmol) in 30 mL of a warm (70°) MeCN/water mixture (1 : 2). The product crystallized upon slow cooling to room temperature, was filtered and washed with small portions of cold water (3 × 20 mL) and dried under vacuum. **1c** was obtained as white crystalline material (0.73 g; 72%). ^{1}H NMR (300 MHz, MeCN-d_3) δ 10.45 (s, 2H, NH), 8.64–8.51 (m, 6H, H$_{PYA}$, H$_{pyr}$), 8.46–8.36 (m, 3H, H$_{PYA}$, H$_{pyr}$), 7.87–7.79 (m, 2H, H$_{PYA}$), 4.29 (s, 6H, N-CH$_3$). ^{13}C NMR (75 MHz, MeCN-d_3) δ 163.1 (CO), 148.1 (C$_{pyr}$), 148.0 (C$_{PYA}$), 147.9 (CH$_{PYA}$), 146.5 (CH$_{PYA}$), 141.9 (CH$_{pyr}$), 128.8 (CH$_{pyr}$), 125.1 (CH$_{PYA}$), 124.7 (CH$_{PYA}$), 45.4 (N-CH$_3$). HR ESI-MS: m/z calculated for C$_{19}$H$_{19}$O$_2$N$_5$F$_6$P [M − PF$_6$]$^+$ = 494.1151; found: 494.12. Elemental analysis: anal. calculated for C$_{19}$H$_{19}$F$_{12}$N$_5$O$_2$P$_2$: C: 35.70; H: 3.00; N: 10.95. Found: C: 36.28; H: 2.95; N: 11.03.

General procedure for compounds 2/3a–c

The respective amounts of the ligands **1a–c** (150 mg, 0.235 mmol, 1 eq.), Na$_2$CO$_3$ (75 mg, 0.705 mmol, 3 eq.) and the MCl$_2$·6H$_2$O salts (28 mg, 0.117 mmol, 0.5 eq.) were dissolved in a H$_2$O/EtOH (1 : 1) mixture (10 mL) and stirred at r.t. for 30 min. The solvents were evaporated under reduced pressure. The crude product was redissolved in MeCN, cooled down to −18 °C and filtered over a pad of Celite to remove sodium salt residues. The final products were obtained upon precipitation/crystallization from Et$_2$O.

Compound 2a: [Co(*para*-PYA)$_2$](PF$_6$)$_2$. According to general procedure starting from **1a** and CoCl$_2$·6H$_2$O, which afforded **2a** as light orange solid (80 mg, 66%). ESI-MS: m/z calculated for [M − PF$_6$]$^+$ = 898.1733; found: 898.1733. Elemental analysis: anal. calculated for C$_{38}$H$_{34}$CoF$_{12}$N$_{10}$O$_4$P$_2$: C: 43.73; H: 3.28; N: 13.42. Found: C: 43.50; H: 3.03; N: 13.85.

Compound 2b: [Co(*meta*-PYA)$_2$](PF$_6$)$_2$. According to general procedure starting from **1b** and CoCl$_2$·6H$_2$O, which afforded **2b** as orange solid (120 mg, 98%). ESI-MS: m/z calculated for [M − PF$_6$]$^+$ = 898.1733; found: 898.1738. Elemental analysis: anal. calculated for C$_{38}$H$_{34}$CoF$_{12}$N$_{10}$O$_4$P$_2$·H$_2$O: C: 42.99; H: 3.42; N: 13.19. Found: C: 43.05; H: 4.20; N: 13.44.

Compound 2b$^+$: [Co(*meta*-PYA)$_2$](PF$_6$)$_3$. A saturated solution of complex **2b** in H$_2$O or D$_2$O was left standing for 3 days which resulted in the formation of green crystals. The solvent was removed and the crystals washed with cold water and Et$_2$O and dried in air to give **2b$^+$** (in H$_2$O) or **2b$^+$-*d*$_8$** (in D$_2$O).

2b$^+$: ESI-MS: m/z calculated for [M − PF$_6$]$^+$ = 1043.1375; found: 1043.1393. ^{1}H NMR (300 MHz, MeCN-d_3): δ 8.39 (t, $^3J_{HH}$ = 7.7 Hz, 2H, H$_{pyr}$), 8.27–8.22 (m, 4H, H$^6_{PYA}$), 8.15 (d, $^3J_{HH}$ = 7.7 Hz, 4H, H$_{pyr}$), 8.11 (s, 4H, H$^2_{PYA}$), 7.62–7.56 (m, 8H, H$^{4/5}_{PYA}$), 4.09 (s, 12H, N-CH$_3$) ppm.

2b$^+$-*d*$_8$: ESI-MS: m/z calculated for [M − PF$_6$]$^+$ = 1051.1877; found: 1051.1883. ^{1}H NMR (300 MHz, MeCN-d_3): δ 8.39 (t, $^3J_{HH}$ = 7.7 Hz, 2H, H$_{pyr}$), 8.15 (d, $^3J_{HH}$ = 7.7 Hz, 4H, H$_{pyr}$), 7.61–7.56 (m, 8H, H$^{4/5}_{PYA}$), 4.10 (s, 12H, N-CH$_3$) ppm.

Compound 2c: [Co(*ortho*-PYA)$_2$](PF$_6$)$_2$. According to general procedure starting from **1c** and CoCl$_2$·6H$_2$O, which afforded **2c** as red solid (115 mg, 94%). ESI-MS: m/z calculated for [M − PF$_6$]$^+$ = 898.1733; found: 898.1724. Elemental analysis: anal. calculated for C$_{38}$H$_{34}$CoF$_{12}$N$_{10}$O$_4$P$_2$: C: 43.73; H: 3.28; N: 13.42. Found: C: 42.22; H: 2.57; N: 13.51. Despite several attempts, no better microanalytical data were obtained. The irregular values may be associated with partial oxidation of the compound.

Compound 3a: [Ni(*para*-PYA)$_2$](PF$_6$)$_2$. According to general procedure starting from **1a** and NiCl$_2$·6H$_2$O, which afforded **3a** as bright yellow solid (78 mg, 64%). ESI-MS: m/z calculated for [M − PF$_6$]$^+$ = 897.1754; found: 897.1730. Elemental analysis: anal. calculated for C$_{38}$H$_{34}$NiF$_{12}$N$_{10}$O$_4$P$_2$·0.5H$_2$O·0.5MeCN: C: 43.66; H: 3.43; N: 13.71. Found: C: 43.40; H: 3.03; N: 14.15.

Compound 3b: [Ni(*meta*-PYA)$_2$](PF$_6$)$_2$. According to general procedure starting from **1b** and NiCl$_2$·6H$_2$O, which afforded **3b** as dark yellow solid (115 mg, 95%). ESI-MS: m/z calculated for [M − PF$_6$]$^+$ = 897.1754; found: 897.1758. Elemental analysis: anal. calculated for C$_{38}$H$_{34}$NiF$_{12}$N$_{10}$O$_4$P$_2$·1.5H$_2$O: C: 42.64; H: 3.48; N: 13.09. Found: C: 42.61; H: 4.09; N: 13.35.

Compound 3c: [Ni(*ortho*-PYA)$_2$](PF$_6$)$_2$. According to general procedure starting from **1c** and NiCl$_2$·6H$_2$O, which afforded **3c** as yellow/green solid (75 mg, 61%). ESI-MS: m/z calculated for

Open Access Article. Published on 31 1399. Downloaded on 28/06/1403 06:59:18 ..
This article is licensed under a Creative Commons Attribution 3.0 Unported Licence.

$[M - PF_6]^+$ = 897.1754; found: 897.1737. Elemental analysis: anal. calculated for $C_{38}H_{34}NiF_{12}N_{10}O_4P_2{\cdot}H_2O{\cdot}MeCN$: C: 43.58; H: 3.57; N: 13.98. Found: C: 43.14; H: 3.09; N: 14.04.

General procedure for compounds 4/5a–c

The respective amounts of the ligands **1a–c** (102 mg, 0.16 mmol, 1 eq.) and Na_2CO_3 (45 mg, 0.42 mmol, 3 eq.) were dissolved in DMF (4 mL) and stirred for 20 min at r.t. In a second vial the $MCl_2{\cdot}6H_2O$ salts (38 mg, 0.16 mmol, 1 eq.) were dissolved in DMF (4 mL). The ligand solution was filtered and slowly added to the metal solution. The combined reaction phase was stirred for another 2 h at r.t. and the final products were obtained upon precipitation/crystallization from Et_2O and MeCN/Et_2O.

Compound 4a: [Co(*para*-PYA)Cl$_2$]. According to general procedure starting from **1a** and $CoCl_2{\cdot}6H_2O$, which afforded **4a** as light green solid (33 mg, 43%). ESI-MS: *m*/*z* calculated for $[M - Cl]^+$ = 441.0403; found: 441.0409. Elemental analysis: anal. calculated for $C_{19}H_{17}Cl_2CoN_5O_2$: C: 47.82; H: 3.59; N: 14.68. Found: C: 47.91; H: 3.31; N: 15.04.

Compound 4b: [Co(*meta*-PYA)Cl$_2$]. According to general procedure starting from **1b** and $CoCl_2{\cdot}6H_2O$, which afforded **4b** as turquoise solid (35 mg, 46%). ESI-MS: *m*/*z* calculated for $[M - Cl]^+$ = 441.0403; found: 441.0407. Elemental analysis: anal. calculated for $C_{19}H_{17}Cl_2CoN_5O_2{\cdot}0.5MeCN$: C: 48.26; H: 3.74; N: 15.48. Found: C: 48.21; H: 3.36; N: 15.30.

Compound 4c: [Co(*ortho*-PYA)Cl$_2$]. According to general procedure starting from **1c** and $CoCl_2{\cdot}6H_2O$, which afforded **4c** as forest green solid (43 mg, 56%). ESI-MS: *m*/*z* calculated for $[M - Cl]^+$ = 441.0403; found: 441.0406. Elemental analysis: anal. calculated for $C_{19}H_{17}Cl_2CoN_5O_2$: C: 47.82; H: 3.59; N: 14.68. Found: C: 47.85; H: 3.55; N: 14.76.

Compound 5a: [Ni(*para*-PYA)Cl$_2$]. According to general procedure starting from **1a** and $NiCl_2{\cdot}6H_2O$, which afforded **5a** as yellow/orange solid (31 mg, 41%). ESI-MS: *m*/*z* calculated for $[M - Cl]^+$ = 440.0424; found: 440.0410. Elemental analysis: anal. calculated for $C_{19}H_{17}Cl_2NiN_5O_2{\cdot}0.5H_2O$: C: 46.96; H: 3.73; N: 14.41. Found: C: 47.29; H: 4.13; N: 14.75.

Compound 5b: [Ni(*meta*-PYA)Cl$_2$]. According to general procedure starting from **1b** and $NiCl_2{\cdot}6H_2O$, which afforded **5b** as yellow solid (39 mg, 51%). ESI-MS: *m*/*z* calculated for $[M - Cl]^+$ = 440.0424; found: 440.0407. Elemental analysis: anal. calculated for $C_{19}H_{17}Cl_2NiN_5O_2$: C: 47.85; H: 3.59; N: 14.68. Found: C: 47.68; H: 3.70; N: 14.41.

Compound 5c: [Ni(*ortho*-PYA)Cl$_2$]. According to general procedure starting from **1c** and $NiCl_2{\cdot}6H_2O$, which afforded **5c** as green solid (42 mg, 55%). ESI-MS: *m*/*z* calculated for $[M - Cl]^+$ = 440.0424; found: 440.0410. Elemental analysis: anal. calculated for $C_{19}H_{17}Cl_2NiN_5O_2$: C: 47.85; H: 3.59; N: 14.68. Found: C: 47.72; H: 3.73; N: 14.31.

General procedure for compounds 6a–c

The respective amounts of ligands **1a–c** (100 mg, 0.16 mmol, 1 eq.) were reacted with Na_2CO_3 (85 mg, 0.80 mmol, 5 eq.) in MeCN (5 mL) for 1 h at room temperature in a vial. Then a 0.2 M $ZnCl_2$ solution in MeCN (470 μL, 0.09 mmol, 0.55 eq.) was added to the ligand solution. The vial was sealed and heated up to 50 °C for 16 h under constant stirring. The reaction mixture was cooled to r.t. and filtered through Celite. A white solid was precipitated from Et_2O (20 mL). The solid was collected by filtration over a fritted funnel, rinsed with Et_2O (3 × 5 mL) and dried.

Compound 6a: [Zn(*para*-PYA)$_2$](PF$_6$)$_2$. According to general procedure starting from **1a** and giving complex **6a** as a white solid (47 mg, 54% yield). ^{1}H NMR (300 MHz, MeCN-d_3): δ 8.47–8.24 (m, 3H, H_{Pyr}), 7.77 (d, $^3J_{HH}$ = 7.3 Hz, 4H, H_{PYA}), 7.22 (d, $^3J_{HH}$ = 7.3 Hz, 4H, H_{PYA}), 3.88 (s, 6H, N-CH_3) ppm. ^{13}C NMR (75 MHz, MeCN-d_3): δ 166.73 (CO), 165.14 (C_{PYA}), 149.89 (C_{Pyr}), 143.73 (CH_{PYA}), 143.35 (CH_{Pyr}), 125.90 (CH_{Pyr}), 120.89 (CH_{PYA}), 46.13 (N-CH_3) ppm. ESI-MS: *m*/*z* calculated for $[M - PF_6]^+$ 903.1698; found: 903.1674. Elemental analysis: anal. calculated for $C_{38}H_{34}F_{12}N_{10}O_4P_2Zn{\cdot}2H_2O$: C: 42.02; H: 3.53; N: 12.90. Found: C: 42.03; H: 3.18; N: 12.80.

Compound 6b: [Zn(*meta*-PYA)$_2$](PF$_6$)$_2$. According to general procedure starting from **1b** and giving complex **6b** as a white solid (46 mg, 55% yield). ^{1}H NMR (300 MHz, MeCN-d_3): δ 8.43 (s, 2H, H_{PYA}), 8.29–8.18 (m, 3H, H_{Pyr}), 7.88 (d, $^3J_{HH}$ = 5.9 Hz, 2H, H_{PYA}), 7.77 (d, $^3J_{HH}$ = 8.5 Hz, 2H, H_{PYA}), 7.38 (dd, $^3J_{HH}$ = 8.5, 5.9 Hz, 2H, H_{PYA}), 3.97 (s, 6H, N-CH_3) ppm. ^{13}C NMR (75 MHz, MeCN-d_3): δ 165.61 (CO), 151.40 (C_{PYA}), 150.59 (C_{Pyr}), 143.43 (CH_{Pyr}), 140.48 (CH_{PYA}), 139.66 (CH_{PYA}), 137.10 (CH_{PYA}), 127.66 (CH_{PYA}), 124.93 (CH_{Pyr}), 48.95 (N-CH_3) ppm. ESI-MS: *m*/*z* calculated for $[M - PF_6]^+$ 903.1698; found: 903.1680. Elemental analysis: anal. calculated for $C_{38}H_{34}F_{12}N_{10}O_4P_2Zn{\cdot}2H_2O$: C: 42.02; H: 3.53; N: 12.90. Found: C: 41.95; H: 3.23; N: 12.75.

Compound 6c: [Zn(*ortho*-PYA)$_2$](PF$_6$)$_2$. According to general procedure starting from **1c** and giving complex **6c** as a white solid (72 mg, 80% yield). ^{1}H NMR (300 MHz, MeCN-d_3): δ 8.70 (d, $^3J_{HH}$ = 7.8 Hz, 2H, H_{Pyr}), 8.41 (t, $^3J_{HH}$ = 7.8 Hz, 1H, H_{Pyr}), 8.11 (dd, $^{3/4}J_{HH}$ = 6.5, 1.7 Hz, 2H, H_{PYA}), 8.06 (d, $^3J_{HH}$ = 8.7 Hz, 2H, H_{PYA}), 7.85 (dt, $^{3/4}J_{HH}$ = 7.9, 1.7 Hz, 2H, H_{PYA}), 7.08 (dt, $^3J_{HH}$ = 6.8, 1.4 Hz, 2H, H_{PYA}), 4.02 (s, 6H, N-CH_3) ppm. ^{13}C NMR (75 MHz, MeCN-d_3) δ 166.38 (CO), 159.57 (C_{PYA}), 150.23 (C_{Pyr}), 144.20 (CH_{PYA}), 143.86 (CH_{Pyr}), 143.51 (CH_{PYA}), 127.03 (CH_{Pyr}), 122.96 (CH_{PYA}), 118.0 (CH_{PYA}), 43.60 (CH_3) ppm. ESI-MS: *m*/*z* calculated for $[M - PF_6]^+$ 903.1698; found: 903.1673. Elemental analysis: anal. calculated for $C_{38}H_{34}F_{12}N_{10}O_4P_2Zn$: C: 43.47; H: 3.26; N: 13.34. Found: C: 42.99; H: 3.16; N: 13.11.

Crystal-structure determination

Suitable single crystals of **2b–c**, **3b–c**, and **4a–c** were mounted in air at ambient conditions and measured on an Oxford Diffraction SuperNova area-detector diffractometer[58] using mirror optics monochromated Mo Kα radiation (λ = 0.71073 Å) and Al filtered.[59] The unit cell constants and an orientation matrix for data collection were obtained from a least-squares refinement of the setting angles of reflections. Data reduction was performed using the CrysAlisPro[58] program. The intensities were corrected for Lorentz and polarization effects, and a numerical absorption correction based on Gaussian inte-

Open Access Article. Published on 31 1399. Downloaded on 28/06/1403 06:59:18 ..
This article is licensed under a Creative Commons Attribution 3.0 Unported Licence.

gration over a multifaceted crystal model was applied. The structure was solved by direct methods using SHELXT,[60] which revealed the positions of all non-hydrogen atoms of the title compounds. The non-hydrogen atoms were refined anisotropically. All H-atoms were placed in geometrically calculated positions and refined using a riding model where each H-atom was assigned a fixed isotropic displacement parameter with a value equal to $1.2U_{eq}$ of its parent atom ($1.5U_{eq}$ for methyl groups and water). Refinement of the structure was carried out on F^2 using full-matrix least-squares procedures, which minimized the function $\sum w(F_o^2 - F_c^2)^2$. The weighting scheme was based on counting statistics and included a factor to down-weight the intense reflections. All calculations were performed using the SHELXL-2014/7 [61] program in OLEX2.[62] The PF_6^- anions in the crystals of complex **2b**, **2c**, and **3b** are disordered as indicated by the high residual electron density peak near its P-atom. No conclusive disorder model was found for **2b** and **3b**, while for **2c**, disorders about two sites were restrained by SHELX SIMU and RIGU instructions. Further details are given in Tables S4–S6.† Crystallographic data for all structures have been deposited with the Cambridge Crystallographic Data Centre (CCDC) as supplementary publication numbers 2015875 (**2b**), 2015876 (**2b**$^+$), 2015877 (**2c**), 2015878 (**3b**), 2015879 (**3c**), 2015880 (**4a**), 2015881 (**4b**), 2015882 (**4c**), and 2015883 ([Ru(*ortho*-pyPYA$_2$)(MeCN)$_3$](PF$_6$)$_2$).†

Conflicts of interest

The authors declare no conflict of interest.

Acknowledgements

We acknowledge generous financial support from the European Research Council (CoG 615653) and from the Swiss National Science Foundation (200021_162868 and 200020_182663, R'equip projects 206021_128724 and 206021_170755). We thank the group of Chemical Crystallography of the University of Bern for the X-ray analysis of all reported structures.

References

1 F. Haber and G. van Oordt, *Z. Anorg. Allg. Chem.*, 1905, **44**, 341–378.
2 M. Appl, in *Ullmann's Encyclopedia of Industrial Chemistry*, Wiley-VCH, Weinheim, 2011.
3 *Handbook of Heterogeneous Catalysis*, ed. G. Ertl, H. Knözinger and J. Weitkamp, Wiley-VCH, Weinheim, 2nd edn, 2008.
4 G. F. Froment, *J. Mol. Catal. A: Chem.*, 2000, **163**, 147–156.
5 L. Wang, D. Li, M. Koike, H. Watanabe, Y. Xu, Y. Nakagawa and K. Tomishige, *Fuel*, 2013, **112**, 654–661.
6 J. R. Rostrup-Nielsen, *Catal. Today*, 2000, **63**, 159–164.
7 L. W. Covert and H. Adkins, *J. Am. Chem. Soc.*, 1932, **54**, 4116–4117.
8 H. Adkins and H. R. Billica, *J. Am. Chem. Soc.*, 1948, **70**, 695–698.
9 M. Albrecht and G. Van Koten, *Angew. Chem., Int. Ed.*, 2001, **40**, 3750–3781.
10 B. Su, Z. C. Cao and Z. J. Shi, *Acc. Chem. Res.*, 2015, **48**, 886–896.
11 H. C. Urey, *Rev. Mod. Phys.*, 1952, **28**, 53–74.
12 J. W. Morgan and E. Anders, *Proc. Natl. Acad. Sci. U. S. A.*, 1969, **77**, 6973–6977.
13 P. E. Brubaker, J. P. Moran, K. Bridbord and F. G. Hueter, *Environ. Health Perspect.*, 1975, **10**, 39–56.
14 L. Alig, M. Fritz and S. Schneider, *Chem. Rev.*, 2019, **119**, 2681–2751.
15 I. Bauer and H.-J. Knölker, *Chem. Rev.*, 2015, **115**, 3170–3387.
16 W. Zuo, A. J. Lough, Y. F. Li and R. H. Morris, *Science*, 2013, **342**, 1080–1084.
17 M. Garbe, K. Junge and M. Beller, *Eur. J. Org. Chem.*, 2017, 4344–4362.
18 S. Z. Tasker, E. A. Standley and T. F. Jamison, *Nature*, 2014, **509**, 299–309.
19 P. Melle, Y. Manoharan and M. Albrecht, *Inorg. Chem.*, 2018, **57**, 11761–11774.
20 P. Melle, J. Thiede, D. A. Hey and M. Albrecht, *Chem. – Eur. J.*, 2020, DOI: 10.1002/chem.202001145.
21 P. Melle and M. Albrecht, *Chimia*, 2019, **73**, 299–303.
22 K. F. Donnelly, C. Segarra, L.-X. Shao, R. Suen, H. Müller-Bunz and M. Albrecht, *Organometallics*, 2015, **34**, 4076–4084.
23 V. Leigh, D. J. Carleton, J. Olguin, H. Mueller-Bunz, L. J. Wright and M. Albrecht, *Inorg. Chem.*, 2014, **53**, 8054–8060.
24 K. Salzmann, C. Segarra and M. Albrecht, *Angew. Chem.*, 2020, **59**, 8932–8936.
25 A. Weilhard, K. Salzmann, M. Navarro, J. Dupont, M. Albrecht and V. Sans, *J. Catal.*, 2020, **385**, 1–9.
26 M. Navarro, C. Segarra, P. Tim and M. Albrecht, *Organometallics*, 2020, **39**, 2383–2391.
27 M. Navarro, V. Rosar, T. Montini, B. Milani and M. Albrecht, *Organometallics*, 2018, **37**, 3619–3630.
28 M. Navarro, M. Li, H. Müller-Bunz, S. Bernhard and M. Albrecht, *Chem. – Eur. J.*, 2016, **22**, 6740–6745.
29 M. Navarro, M. Li, S. Bernhard and M. Albrecht, *Dalton Trans.*, 2017, **47**, 659–662.
30 M. Navarro, C. A. Smith, M. Li, S. Bernhard and M. Albrecht, *Chem. – Eur. J.*, 2018, **24**, 6386–6398.
31 M. E. Doster and S. A. Johnson, *Angew. Chem., Int. Ed.*, 2009, **48**, 2185–2187.
32 Q. Shi, R. J. Thatcher, J. Slattery, P. S. Sauari, A. C. Whitwood, P. C. McGowan and R. E. Douthwaite, *Chem. – Eur. J.*, 2009, **15**, 11346–11360.
33 A. Dorazco-González, H. Höpfl, F. Medrano and A. K. Yatsimirsky, *J. Org. Chem.*, 2010, **75**, 2259–2273.
34 A. K. Patra and R. Mukherjee, *Inorg. Chem.*, 1999, **38**, 1388–1393.

 This journal is © The Royal Society of Chemistry 2020

Open Access Article. Published on 31 1399. Downloaded on 28/06/1403 06:59:18 ..
This article is licensed under a Creative Commons Attribution 3.0 Unported Licence.

35 D. Huang and R. H. Holm, *J. Am. Chem. Soc.*, 2010, **132**, 4693–4701.
36 P. Pirovano, E. R. Farquhar, M. Swart and A. R. McDonald, *J. Am. Chem. Soc.*, 2016, **138**, 14362–14370.
37 C. M. A. Muller, M. V. Babak, M. Kubanik, M. Hanif, S. M. F. Jamieson, C. G. Hartinger and L. J. Wright, *Inorg. Chim. Acta*, 2016, **450**, 124–130.
38 With iron and cobalt observed in pyridine dicarboxamide systems, see: (*a*) G. L. Guillet, J. B. Gordon, G. N. Di Francesco, M. W. Calkins, E. Čižmár, K. A. Abboud, M. W. Meisel, R. García-Serres and L. J. Murray, *Inorg. Chem.*, 2015, **54**, 2691–2704; (*b*) T. C. Harrop, L. A. Tyler, M. M. Olmstead and P. K. Mascharak, *Eur. J. Inorg. Chem.*, 2003, 475–481.
39 P. Pirovano, B. Twamley and A. R. McDonald, *Chem. – Eur. J.*, 2018, **24**, 5238–5245.
40 A. W. Addison, T. N. Rao, J. Reedijk, J. van Rijn and G. C. Verschoor, *J. Chem. Soc., Dalton Trans.*, 1984, 1349–1356.
41 E. Goldschmied and N. C. Stephenson, *Acta Crystallogr., Sect. B: Struct. Crystallogr. Cryst. Chem.*, 1970, **26**, 1867–1875.
42 X. Zhang, D. Huang, Y. S. Chen and R. H. Holm, *Inorg. Chem.*, 2012, **51**, 11017–11029.
43 D. Bansal, G. Kumar, G. Hundal and R. Gupta, *Dalton Trans.*, 2014, **43**, 14865–14875.
44 D. Bansal and R. Gupta, *Dalton Trans.*, 2019, **48**, 14737–14747.
45 For examples of κ^3-*O*,*N*,*O* coordination due to grid restrains, see: (*a*) L. K. Thompson, L. Zhao, Z. Xu, D. O. Miller and W. M. Reiff, *Inorg. Chem.*, 2003, **42**, 128–139; (*b*) L. N. Dawe, K. V. Shuvaev and L. K. Thompson, *Inorg. Chem.*, 2009, **48**, 3323–3341.
46 H. Eyring, *J. Chem. Phys.*, 1935, **3**, 107–115.
47 The TC were obtained upon comparing ^{1}H NMR spectra of **6c** recorded in CD_2Cl_2 in the +20 to −80 °C temperature range. The difference of the resonance frequencies ($\delta\nu$) was calculated from chemical shift differences for protons of the major species, *i.e.* bis-(κ^3-*N*,*N*,*N*-pincer), to the average chemical shift of the corresponding protons in the minor species (κ^3-*N*,*N*,*N*/κ^3-*O*,*N*,*O*-isomer). The energy barrier ($\Delta G^{\ddagger}$) between the two isomers was estimated by using the following equation: $\Delta G^{\ddagger} = 4.57 \cdot T_c \cdot (9.97 + \log T_c/\delta\nu)$ according to: H. Günther, *NMR-Spektroskopie*, Thieme, Stuttgart, 1973.
48 M. Hesse, H. Meier and B. Zeeh, *Spektroskopische Methoden in der organischen Chemie*, Thieme, Stuttgart, Germany, 8th edn, 2012.
49 C. M. Harris, T. N. Lockyer, R. L. Martin, R. L. Patil, E. Sinn and I. M. Stewart, *Aust. J. Chem.*, 1969, **22**, 2105–2126.
50 M. Navarro, Doctoral dissertation, University of Bern, 2017.
51 C. Arana, S. Yan, M. Keshavarz-K, K. T. Potts and H. D. Abruña, *Inorg. Chem.*, 1992, **31**, 3680–3682.
52 *Ideal value one electron process is 56.5 mV according to Butler–Volmer equation, experimental values are known to be slightly higher*; T. Erdey-Grúz and M. Volmer, *Z. Phys. Chem.*, 1930, **150**, 203–213.
53 We note that the CV of complex **2a** indicates a second oxidation process at slightly higher potential. This process might be rationalized by a linkage isomerism also in this compound, though we do not have any experimental support for dynamic *O*- *vs.* *N*-coordination of *para*-pyPYA$_2$ ligands.
54 J.-M. Savéant, *Elements of Molecular and Biomolecular Electrochemistry*, John Wiley & Sons, Hoboken, United States, 2006.
55 A. J. Bard and L. R. Faulkner, *Electrochemical Methods: Fundamentaland Applications*, John Wiley & Sons, Hoboken, United States, 2nd edn, 2001.
56 Mesoionic compounds are defined by IUPAC as "dipolar five- (possibly six-) membered heterocyclic compounds in which both the negative and the positive charge are delocalized, for which a totally covalent structure cannot be written, and which cannot be represented satisfactorily by any one polar structure. The formal positive charge is associated with the ring atoms, and the formal negative charge is associated with ring atoms or an exocyclic nitrogen or chalcogen atom". IUPAC. *Compendium of Chemical Terminology, 2nd Ed. Gold Book Compiled* by A. D. McNaught and A. Wilkinson, Blackwell Scientific Publications, Oxford, 1997. XML online corrected version: http://goldbook.iupac.org (2006) created by M. Nic, J. Jirat, and B. Kosata updates compiled by A. Jenkins. ISBN 0-9678550-9-8.
57 N. G. Connelly and W. E. Geiger, *Chem. Rev.*, 1996, **96**, 877–910.
58 Oxford Diffraction Ltd., *CrysAlisPro*, Yarnton, Oxfordshire, U.K., Version 1., 2010.
59 P. Macchi, H.-B. Bürgi, A. S. Chimpri, J. Hauser and Z. Gál, *J. Appl. Crystallogr.*, 2011, **44**, 763–771.
60 G. M. Sheldrick, *Acta Crystallogr., Sect. C: Struct. Chem.*, 2015, **71**, 3–8.
61 G. M. Sheldrick, *Acta Crystallogr., Sect. A: Found. Adv.*, 2015, **71**, 3–8.
62 O. V. Dolomanov, L. J. Bourhis, R. J. Gildea, J. A. K. Howard and H. Puschmann, *J. Appl. Crystallogr.*, 2009, **42**, 339–341.